Supplementary Data

Accommodation of an N-(deoxyguanosin-8-yl)-2-acetylaminofluorene adduct in the active site of human DNA polymerase ι: Hoogsteen or Watson-Crick base pairing?†

*Kerry Donny-Clark‡, Robert Shapiro§, and Suse Broyde‡,**

‡Department of Biology and §Department of Chemistry, New York University, New York, NY, 10003, USA

Running Title: Bypassing a bulky major groove dG-AAF adduct in polι

†This research is supported by NIH CA75449 to S.B. and R.S., and by the National Science Foundation through TeraGrid resources provided by the San Diego Supercomputer Center. Support for computational infrastructure and systems management was also provided by NIH CA28038 to S.B. and R.S. The content is solely the responsibility of the authors and does not necessarily represent the official views of the National Cancer Institute or the National Institutes of Health.

*Corresponding author: Suse Broyde, Tel. (212) 998-8231, Fax (212) 995-4015, Email: broyde@nyu.edu

HG-AAF1 Initial AAF Position

HG-AAF2 Initial AAF Position

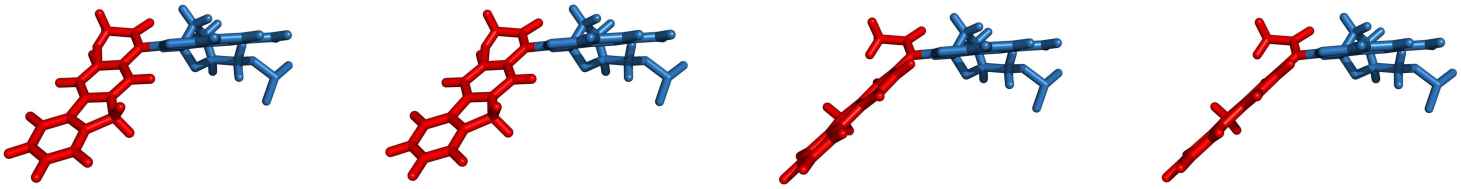

HG-AAF3 Initial AAF Position

HG-AAF4 Initial AAF Position

WC-AAF1 Initial AAF Position

WC-AAF2 Initial AAF Position

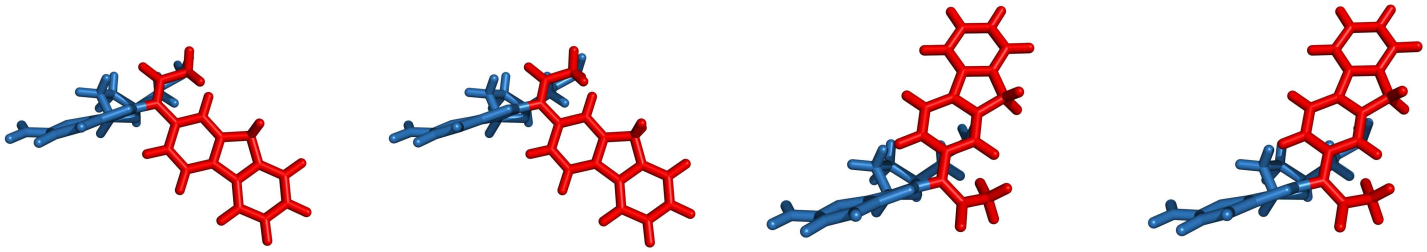

WC-AAF3 Initial AAF Position

WC-AAF4 Initial AAF Position

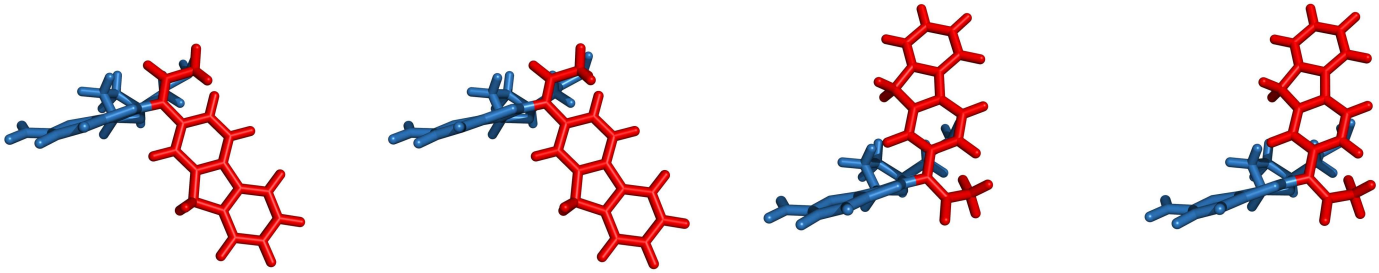

Figure S1: Stereo views of initial conformations of dG-AAF. AAF is red, templating dG is blue.

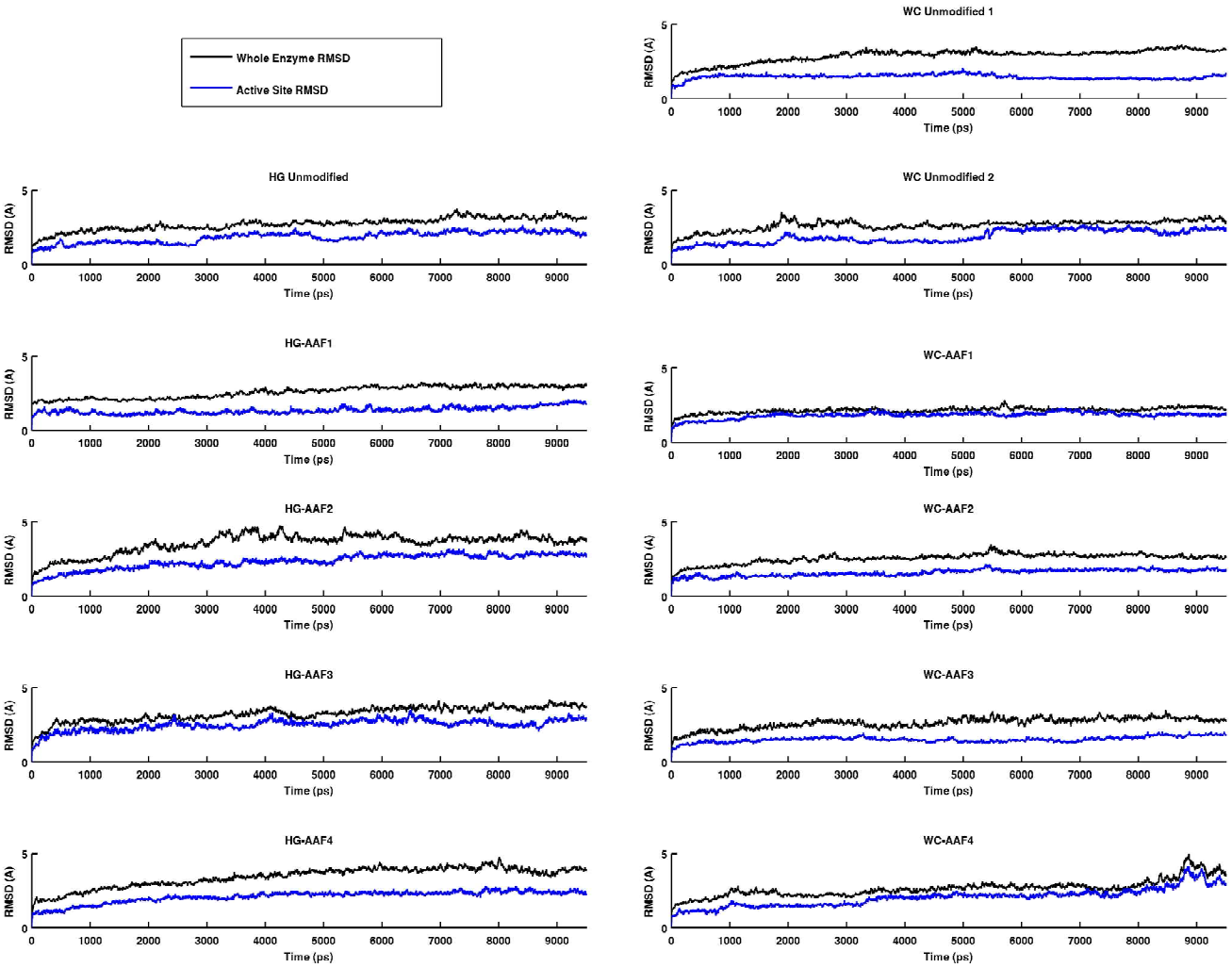

Figure S2: Root mean square deviation (RMSD) of current versus initial structure as a function of time for all 10 ns of each trajectory. All simulations are stable by ~6 ns. For this figure the active site is all residues that have at least one atom within 8Å of any atom in the nascent base pair.

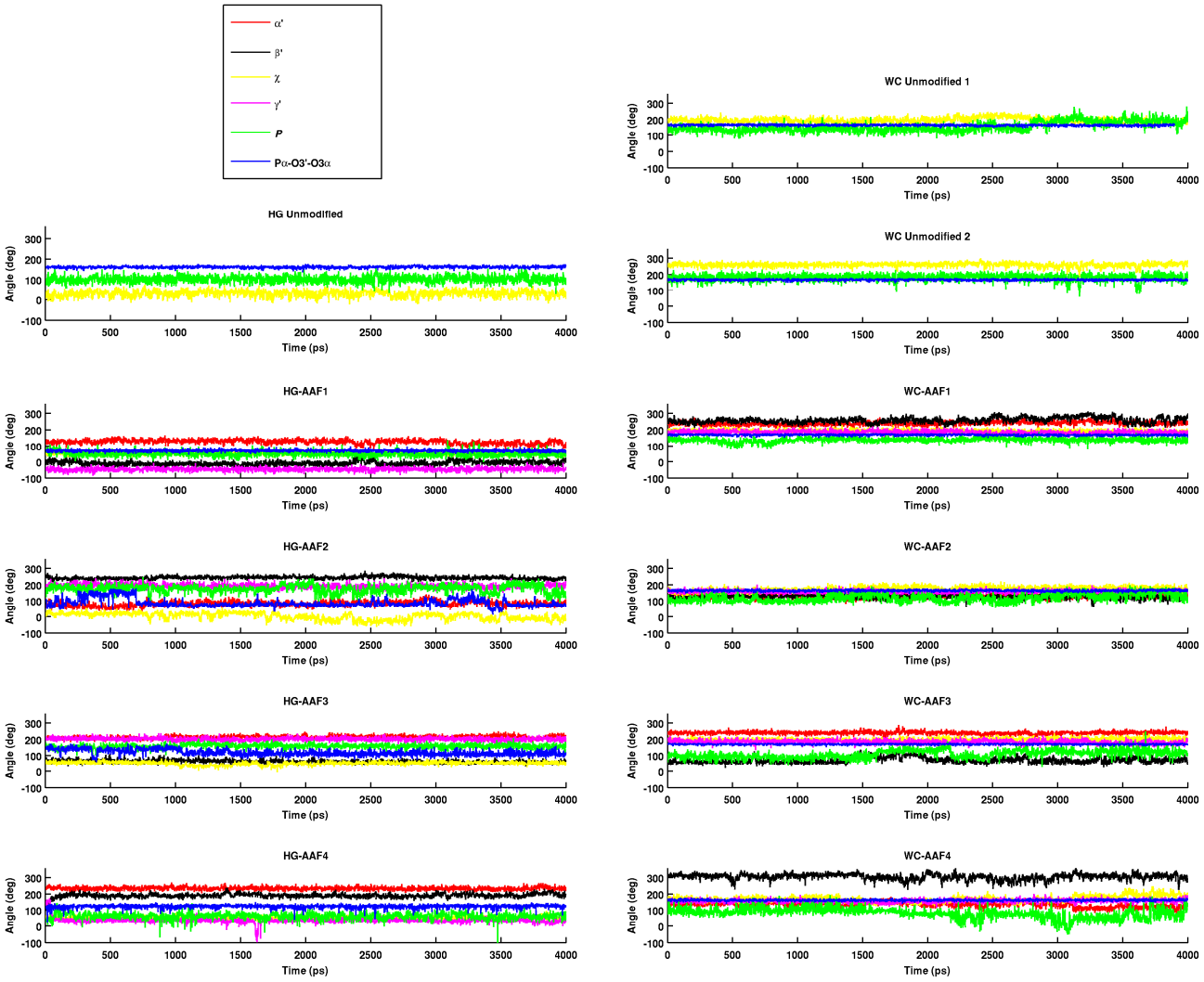

Figure S3: Torsion angles χ, α′, β′, and γ′, the pseudorotation phase angle *P* of the sugar pucker of dG/dG-AAF, and the in-line attack angle O3′- Pα-O3α for the stable region (last 4 ns) of each trajectory versus time.

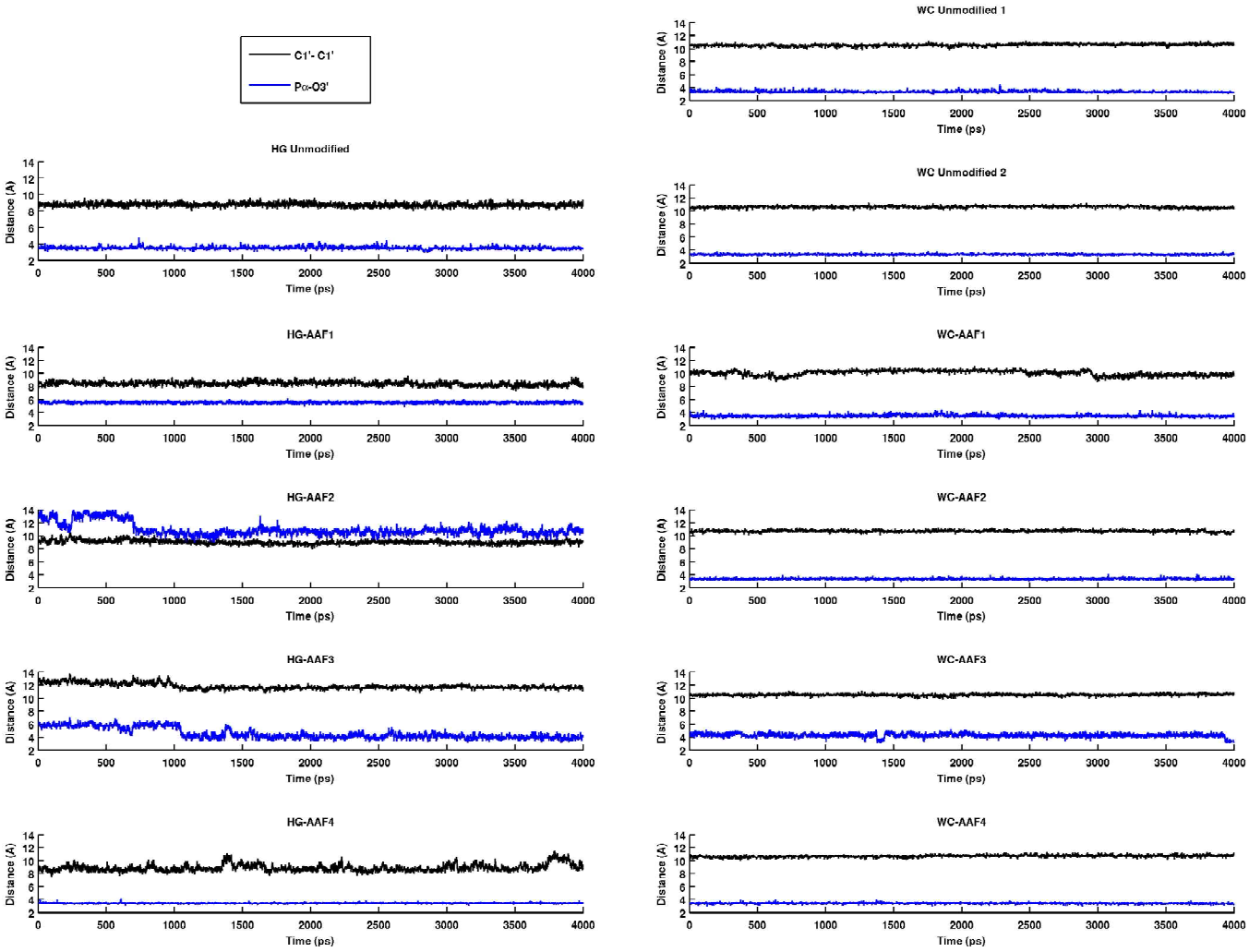

Figure S4: C1′-C1′ and Pα-O3′ distances versus time for the stable region (last 4 ns) of each trajectory.

Unmodified HG Control Stacking

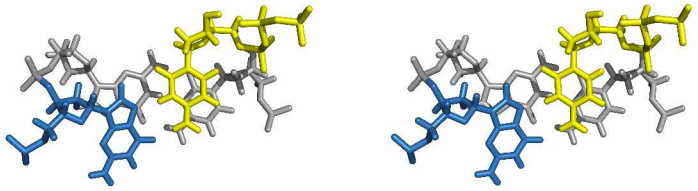

HG-AAF1 Stacking **HG-AAF2 Stacking**

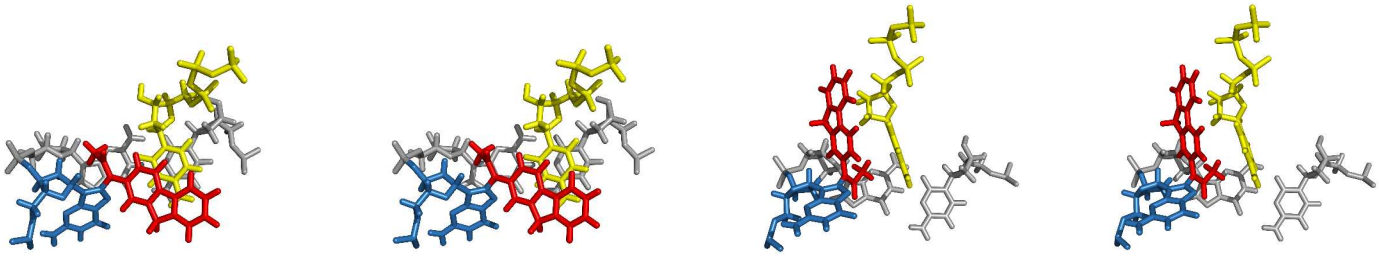

HG-AAF3 Stacking **HG-AAF4 Stacking**

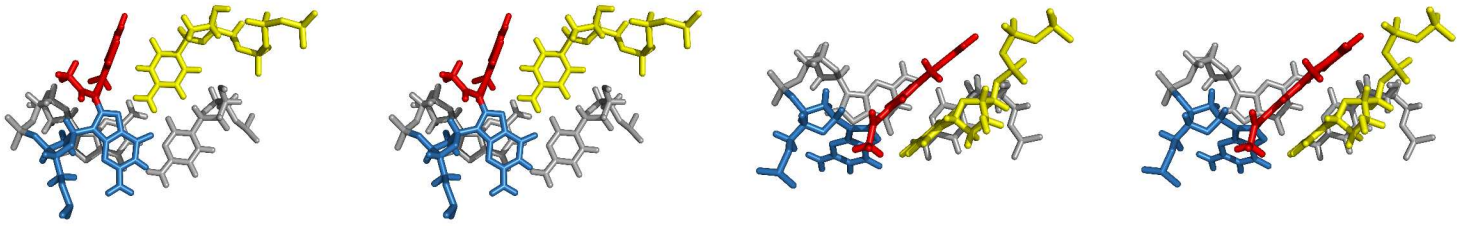

Figure S5: Stereo views of stacking between the nascent base pair and the previously incorporated base pair in the most representative structure. Incoming dCTP$^+$ is yellow, templating dG is blue, AAF is red, and the previously incorporated base pair is gray.

Unmodified WC Control Stacking 1

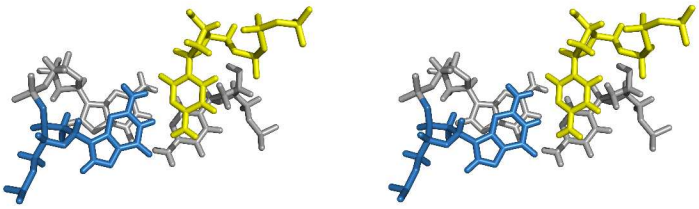

Unmodified WC Control Stacking 2

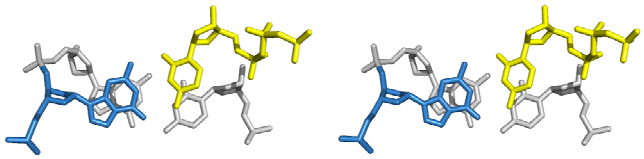

WC-AAF1 Stacking

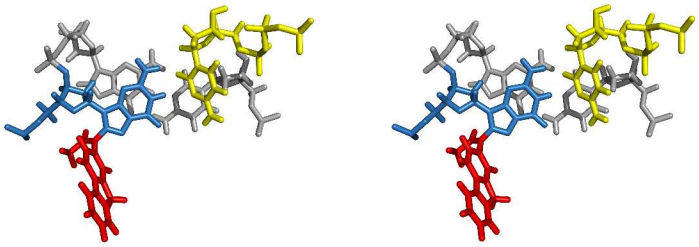

WC-AAF2 Stacking

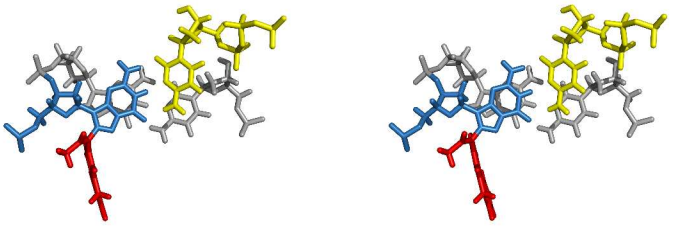

WC-AAF3 Stacking

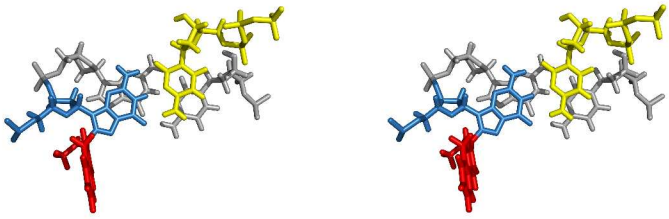

WC-AAF4 Stacking

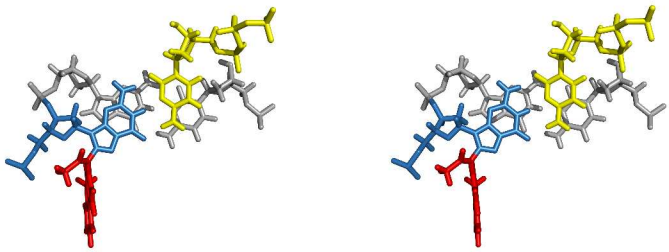

Figure S5 continued: Stereo views of stacking between the nascent base pair and the previously incorporated base pair in the most representative structure. Incoming dCTP is yellow, templating dG is blue, AAF is red, and the previously incorporated base pair is gray.

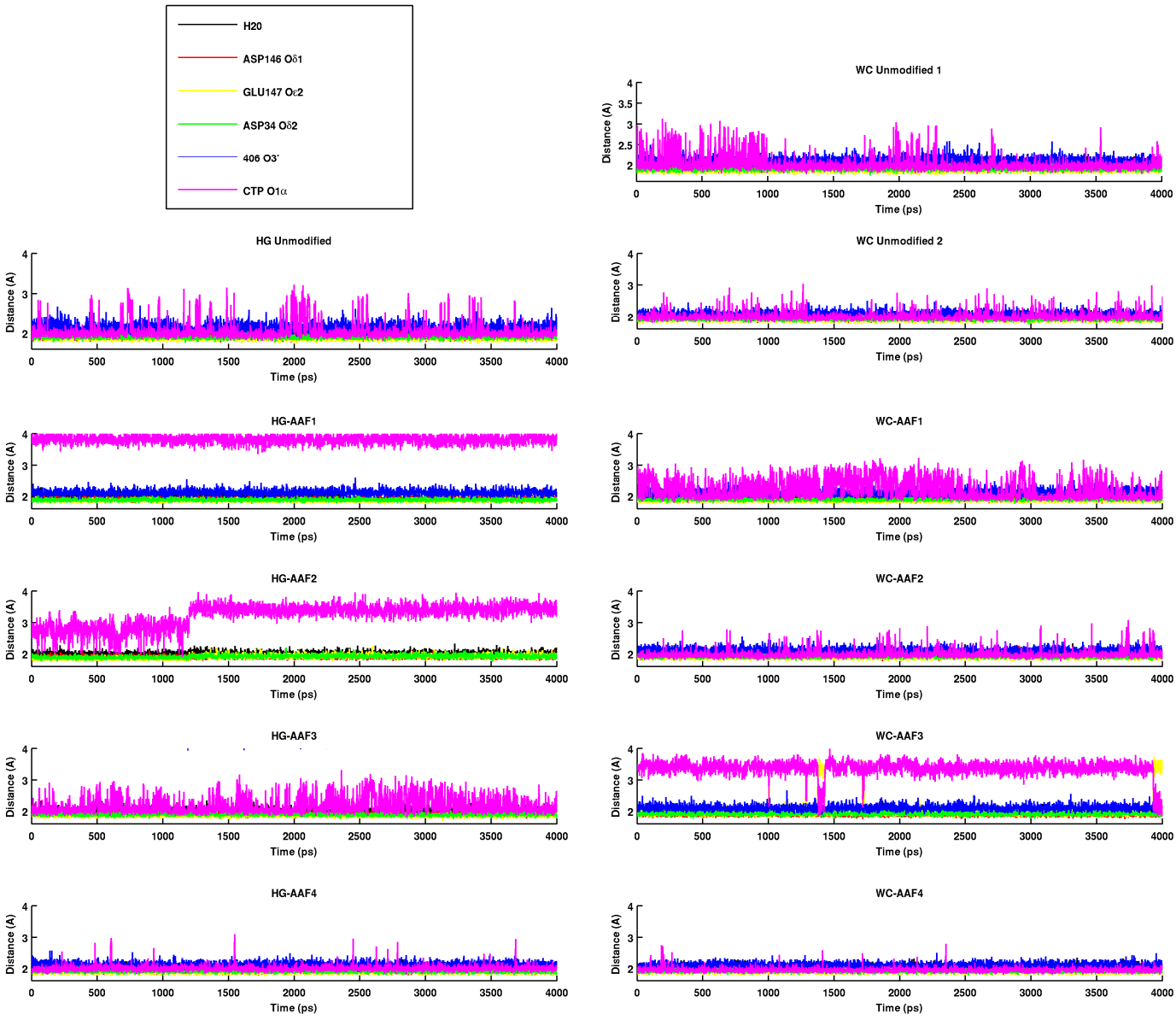

Figure S6: Coordination distances for the catalytic Mg_A^{2+} versus time for the stable region (last 4 ns) of each trajectory.

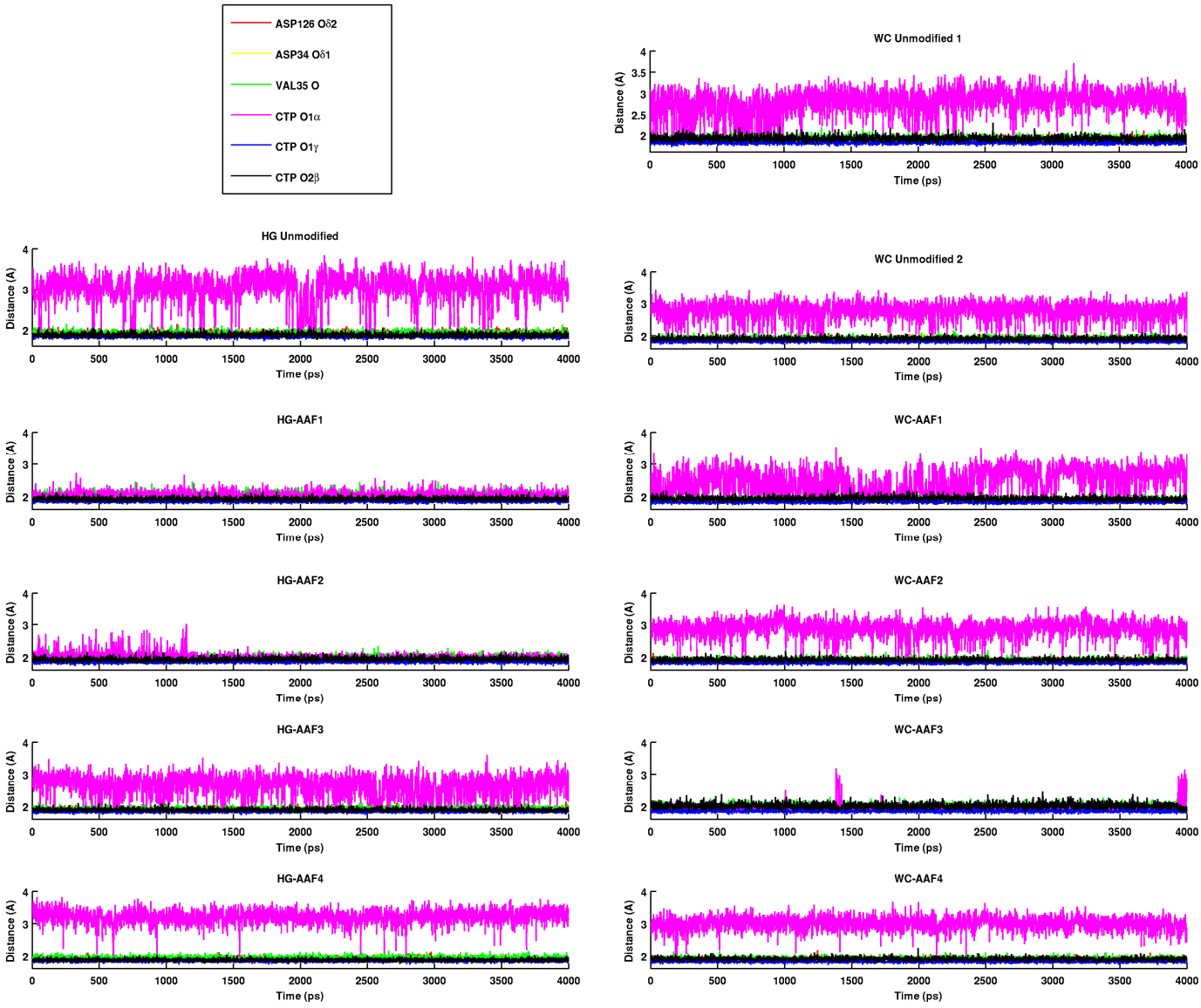

Figure S7: Coordination distances for the nucleotide binding Mg_B^{2+} versus time for the stable region (last 4 ns) of each trajectory.

Unmodified HG Control Active Site

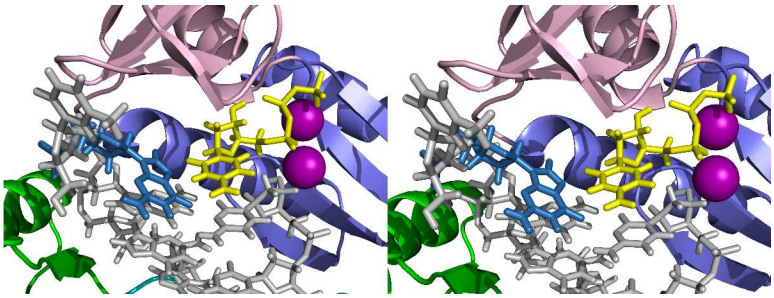

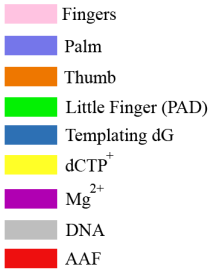

HG-AAF1 Active Site

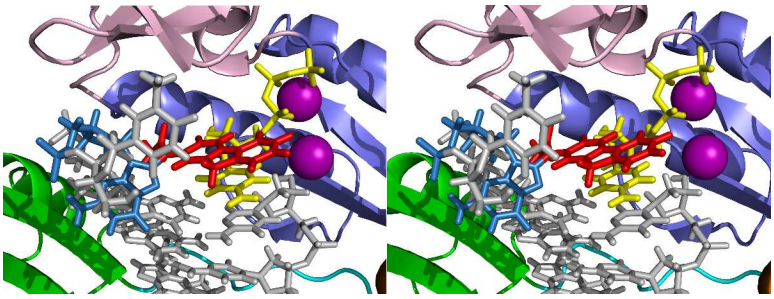

HG-AAF2 Active Site

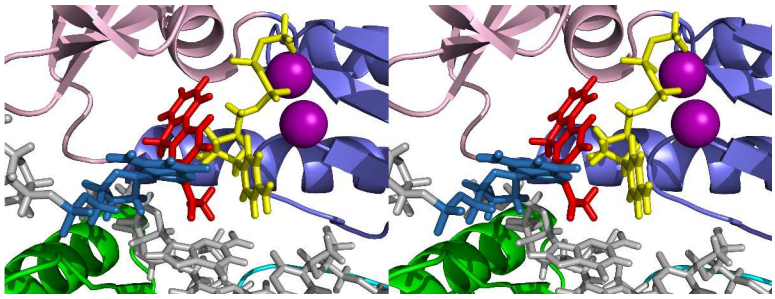

HG-AAF3 Active Site

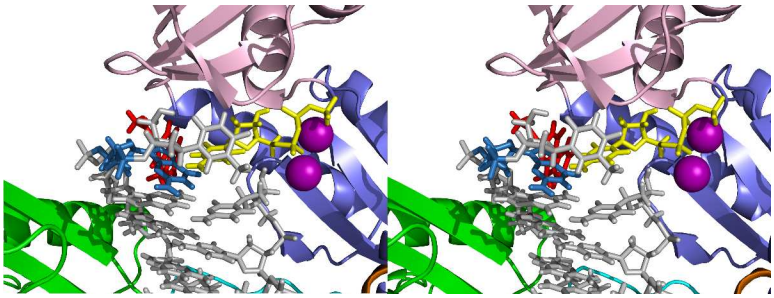

HG- AAF4 Active Site

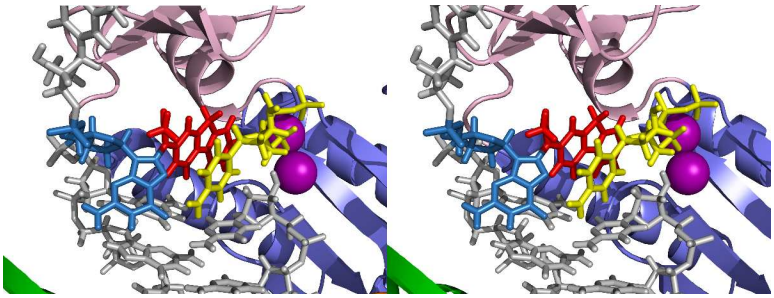

Figure S8: Active site stereo views of the most representative structures for each simulation.

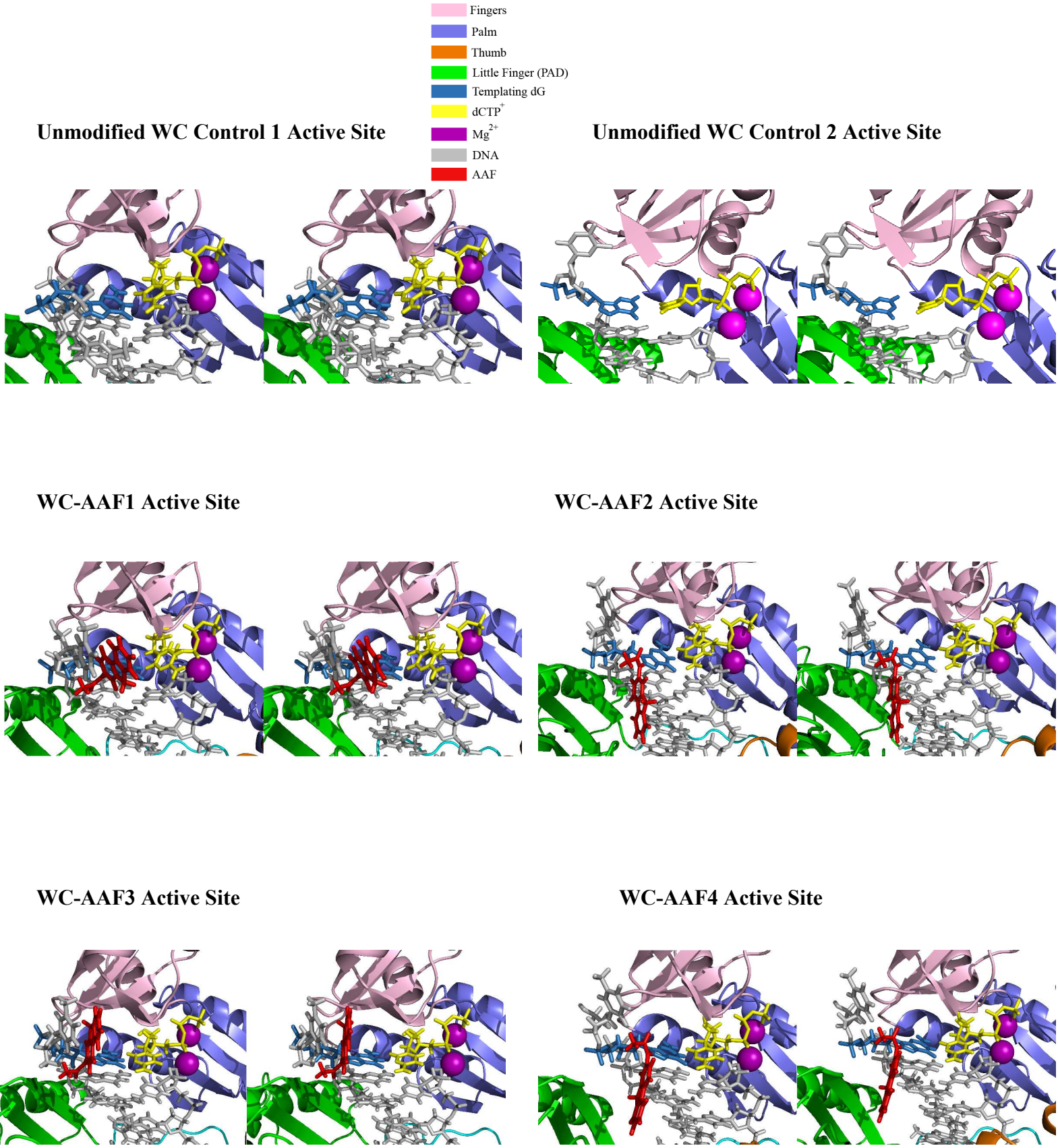

Figure S8 continued: Active site stereo views of the most representative structures for each simulation.

Unmodified HG Control

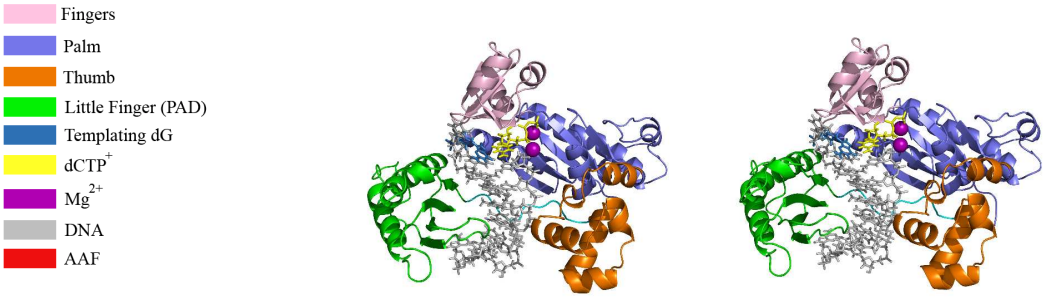

HG-AAF1

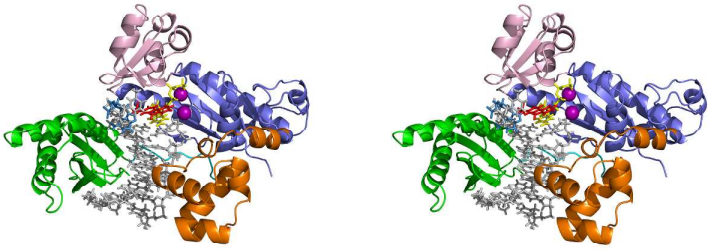

HG-AAF2

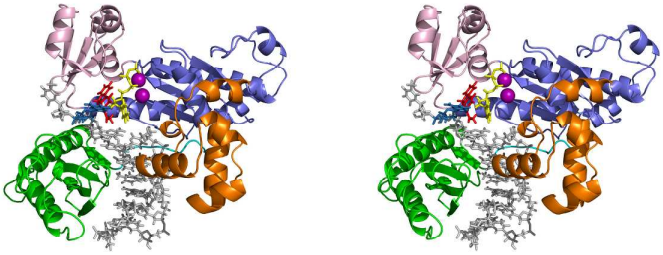

HG-AAF3

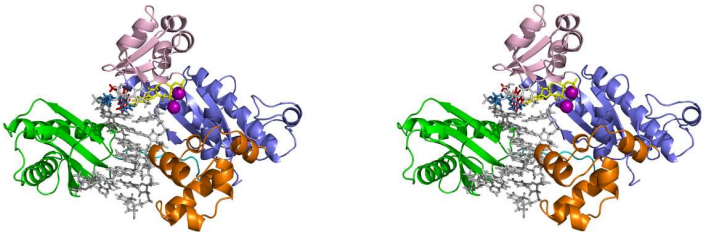

HG-AAF4

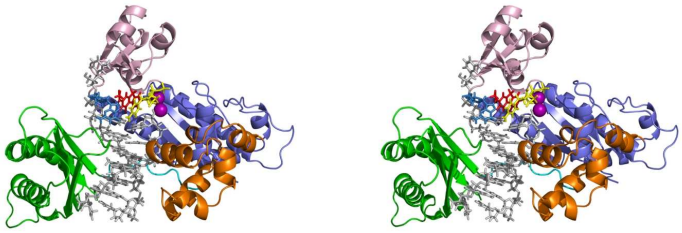

Figure S9: Whole enzyme stereo views of the most representative structures from each trajectory.

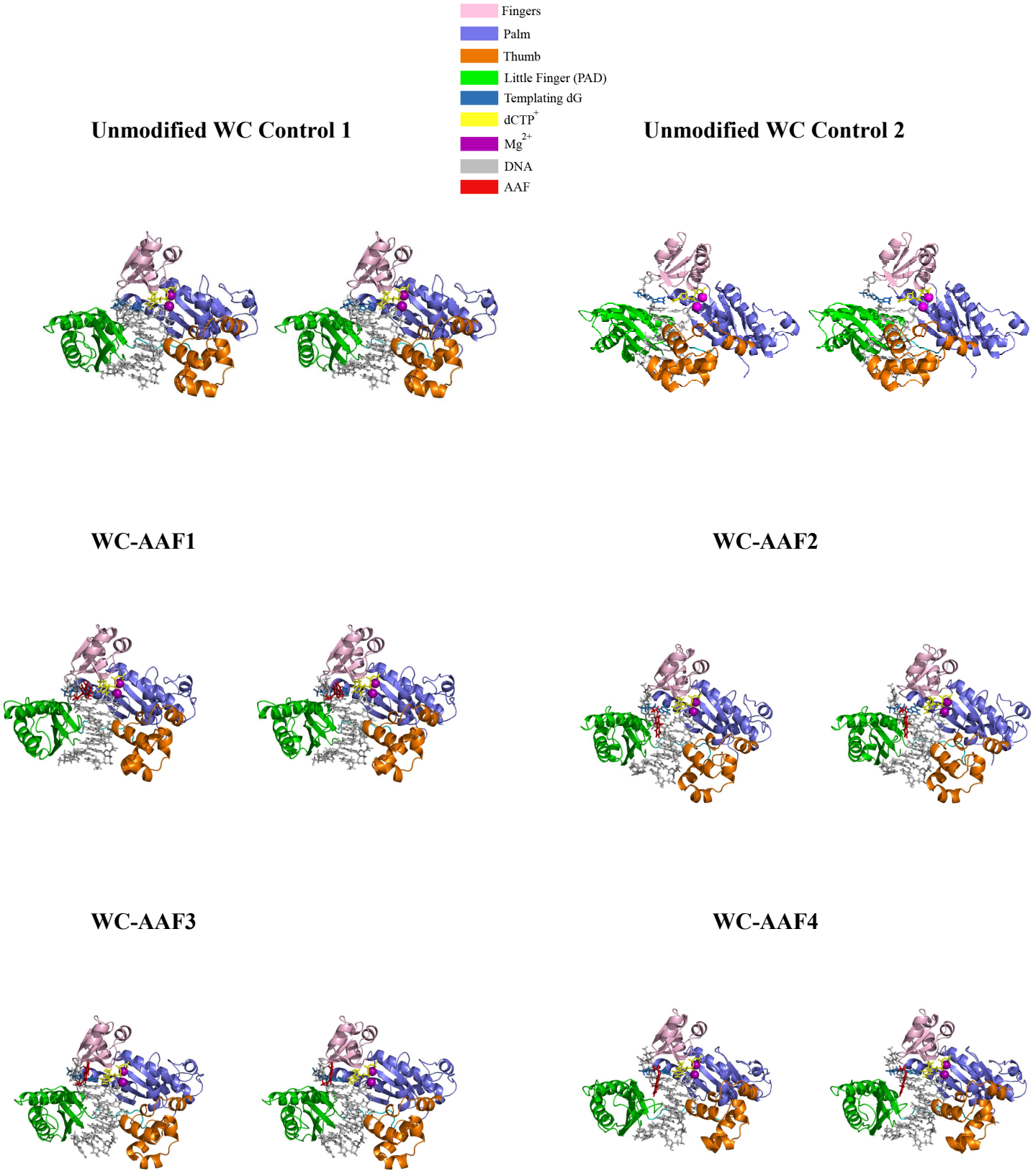

Figure S9 continued: Whole enzyme stereo views of the most representative structures from each trajectory.

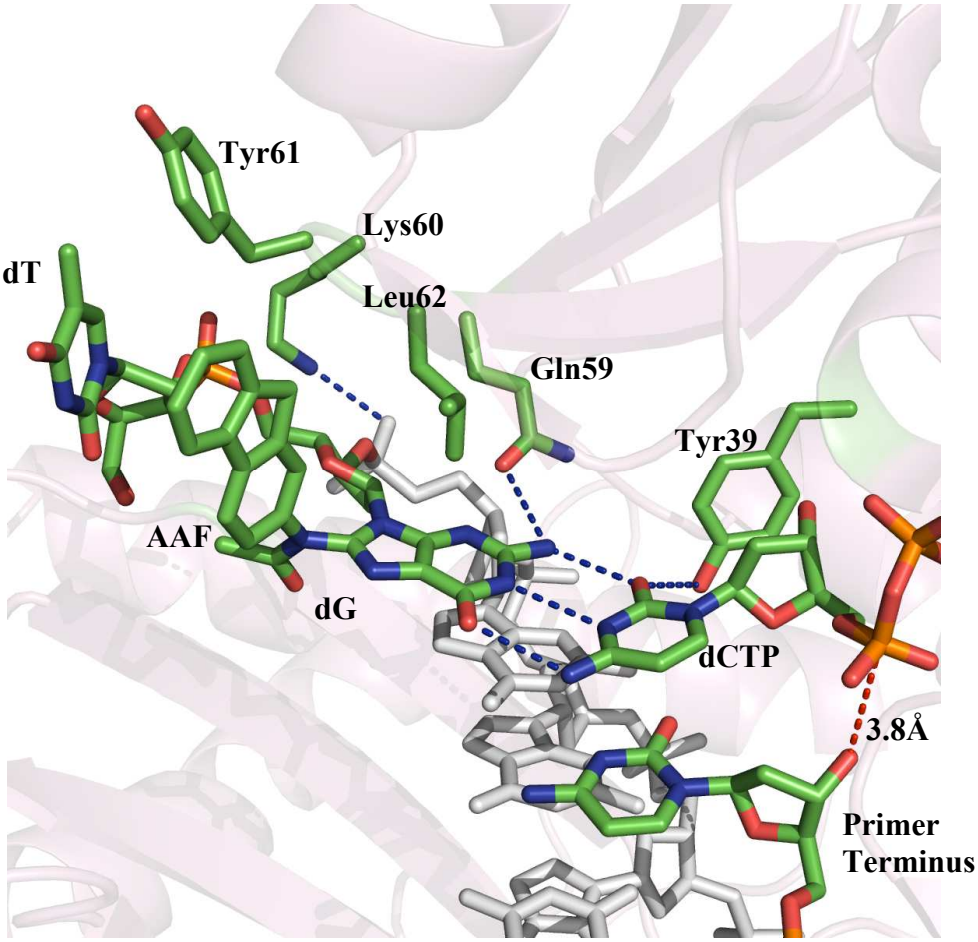

Figure S10: Active site organization and selected hydrogen bonds of WC-AAF3. Polι is pink, duplex DNA is grey, and key active site features are colored by atom. The hydrogen bond between Tyr39 OH and dCTP O3′ brings the dCTP Pα 3.8Å away from the primer terminus O3′. This long Pα-O3′ distance causes the very low near reaction-ready occupancy of this structure. Other features of the active site are similar to the other WC-AAF structures. Oxygen: red; nitrogen: blue; carbon: green; phosphorus: orange.

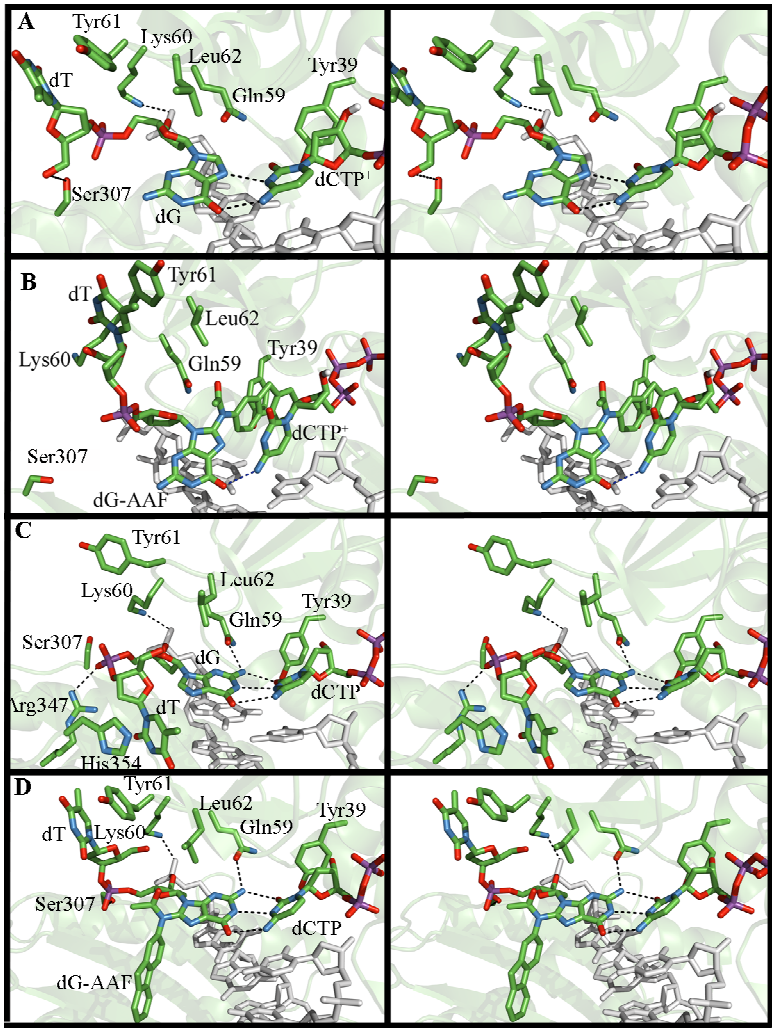

Figure S11: Stereo views of Fig 3 in the main text. Active site organization and hydrogen bonds formed by the templating dG/dG-AAF. Polι is green, duplex DNA is grey, and key active site features are colored by atom. Oxygen: red; nitrogen: blue; carbon: green; phosphorus: purple.

A: Unmodified HG control simulation.

B: HG-AAF4.

C: Unmodified WC control simulation 1.

D: WC-AAF2.